Communication in Physical Sciences, 2026, 13(4): 563-582

Green Synthesis of ZnO Nanoparticles Using Leaf Extract of *Diospyros Mespilifolia and* Its Application

Naseer Inuwa Durumin Iya* Ishak Haladu, Abba Yahaya, Hafiz Ahmad, Fatima Abdulkarim Yunusa, Aminu Bala and Musa Muhammad Bello
Received: 06 September 2025 Accepted: 19 March 2026/Published: 20 April 2026
https://dx.doi.org/10.4314/cps.v13i4.2

Abstract *Zinc oxide nanoparticles (ZnO NPs) were successfully synthesized via a sustainable green route using Diospyros mespiliformis leaf extract as both reducing and capping agent. The formation of ZnO NPs was confirmed by UV–Visible spectroscopy, which exhibited a characteristic excitonic absorption peak at 340 nm, indicating a pronounced blue shift relative to bulk ZnO and an estimated optical bandgap of 3.65 eV. X-ray diffraction (XRD) analysis revealed a highly crystalline, multiphase structure dominated by Zincite (83%), with minor contributions from Gahnite (13%) and Cristobalite (3.8%). The calculated crystallite sizes ranged from 8.6 to 13.7 nm, consistent with nanoscale dimensions and quantum confinement effects. Scanning electron microscopy (SEM) images showed a porous and granular morphology, indicative of a high surface area, while energy-dispersive X-ray (EDX) analysis confirmed the presence of Zn (40.59 wt%) along with a significant sodium content (57.28 wt%) and trace bio-minerals (Ca, K, Si, and Ti) originating from the plant extract. Fourier transform infrared (FTIR) spectroscopy identified key functional groups, particularly hydroxyl (3301 cm^{-1}) and carbonyl groups, which play crucial roles in nanoparticle stabilization and metal ion binding. The adsorption performance of the synthesized ZnO NPs was evaluated for the removal of Pb^{2+} ions from aqueous solutions. Batch adsorption studies demonstrated that removal efficiency is strongly influenced by initial metal ion concentration and solution pH. A maximum removal efficiency of 78.39% was achieved at an initial Pb^{2+} concentration of 0.574 mg/L, while optimal performance was observed under alkaline conditions, reaching 83.8% removal at pH 10.3. The enhanced adsorption capacity is attributed to the high surface-to-volume ratio, porous morphology, surface functionalization, and defect-rich crystalline structure of the nanoparticles. Overall, the results highlight the potential of these green-synthesized ZnO nanoparticles as efficient, eco-friendly, and scalable nano-adsorbents for heavy metal remediation in contaminated water systems.*

Keywords: *Diospyros Mespiliftmis, UV – Visible spectroscopy, Scanning electron microscope, XRD, FTIR*

Naseer Inuwa Durumin Iya*
Address: Department of Chemistry, Faculty of Physical Sciences, Federal University Dutse, P.M.B. 7156, Ibrahim Aliyu Bye-Pass, Dutse, Nigeria
Email: nasduruminiya@fud.edu.ng
https://orcid.org/0009-0002-7938-0191

Ishak Haladu
Address: Department of Chemistry, Faculty of Physical Sciences, Federal University Dutse, P.M.B. 7156, Ibrahim Aliyu Bye-Pass, Dutse, Nigeria
Email: isyakuh2024@yahoo.com

Abba Yahaya
Address: Department of Chemistry, Faculty of Physical Sciences, Federal University Dutse, P.M.B. 7156, Ibrahim Aliyu Bye-Pass, Dutse, Nigeria
Email: abbayahaya@fud.edu.ng
https://orcid.org/0009-0006-0013-5556

Hafiz Ahmad
Address: Department of Chemistry, Faculty of Physical Sciences, Federal University Dutse, P.M.B. 7156, Ibrahim Aliyu Bye-Pass, Dutse,

Nigeria
Email: hafizahmadrng@gmail.com
https://orcid.org/0009-0005-7905-4136

Fatima Abdulkarim Yunusa
Address: Department of Chemistry, Faculty of Physical Sciences, Federal University Dutse, P.M.B. 7156, Ibrahim Aliyu Bye-Pass, Dutse, Nigeria
Email: fateeabdulkarim@mail.com

Musa Muhammad Bello
Address: Department of Chemistry, Faculty of Physical Sciences, Federal University Dutse, P.M.B. 7156, Ibrahim Aliyu Bye-Pass, Dutse, Nigeria
Email: musamuhammadbello1040@gmail.com
https://orcid.org/0009-0004-4435-326X

Aminu Bala
Address: Department of Chemistry, Faculty of Physical Sciences, Federal University Dutse, P.M.B. 7156, Ibrahim Aliyu Bye-Pass, Dutse, Nigeria
Email: balaaminu26@gmail.com

1.0 Introduction

In recent decades, nanotechnology has emerged as a rapidly advancing field due to the unique physicochemical properties exhibited by materials at the nanoscale. Their exceptional properties at the nanoscale, which are strongly influenced by particle size and morphology, make them highly appealing (Fouda *et al.,* 2023; Izein, 2024). Nanotechnology enables the production of nanoparticles with unique features, including low density, high specific surface area, enhanced catalytic efficiency, and notable electrical, optical, antimicrobial, mechanical, and magnetic properties (Prashanth *et al.,* 2024; Jadhav *et al.,* 2024). These attributes have driven significant progress in medicine, engineering, and technological innovation (Karan *et al.,* 2024). In addition, nanotechnology has contributed to advancements in agriculture by improving seed germination and plant growth (Asmat-Campos *et al.,* 2022), environmental remediation through wastewater treatment (Abegunde *et al*., 2024), and the energy sector by enhancing the efficiency of solar cells (Yang *et al.,* 2023). Conventional nanoparticle synthesis techniques often rely on costly and environmentally harmful physicochemical approaches (Azizi *et al.,* 2014). Physical synthesis methods typically require sophisticated equipment and extreme operating conditions, whereas chemical methods involve the use of toxic reagents and generate hazardous by-products, thereby restricting their applicability in biomedical and food-related fields (Muresan *et al.,* 2024). In contrast, green synthesis methods that utilize biological resources have emerged as sustainable and effective alternatives (Sugitha *et al.*, 2024). These eco-friendly approaches employ plants, microorganisms, and agricultural waste to produce stable and multifunctional nanomaterials (Battacharjee *et al.,* 2024). Meanwhile, infectious diseases continue to represent a significant public health challenge, worsened by the growing resistance of pathogenic bacteria to standard antibiotics due to their misuse and overuse, including methicillin-resistant *Staphylococcus aureus* and vancomycin-resistant *Enterococcus* (Muresan *et al*., 2024; Sugitha *et al.,* 2024; Battacharjee *et al*., 2024; Morowvat *et al.,* 2024). Such antibiotic-resistant infections, prevalent in both community and hospital environments, impose substantial financial burdens on healthcare systems worldwide (Morowvat *et al*., 2024).

Nanotechnology has emerged as a promising and safe approach in the urgent search for novel and effective antimicrobial agents capable of destroying and suppressing microbial growth, as its mode of action differs fundamentally from that of conventional antibiotics (Salayova

et al., 2021). Metal and metal oxide nanoparticles have therefore attracted considerable attention for a wide range of biological applications (Eddy *et* al., 2023a; Seghir *et al*., 2023). Beyond biomedical applications, ZnO nanoparticles have also demonstrated strong potential in environmental remediation, particularly in pollutant adsorption.

They are particularly notable due to their distinctive properties, including a wide direct band gap of 3.37 eV, high exciton binding energy (60 meV), strong room-temperature luminescence, excellent thermal stability, superior mechanical strength, high photostability, and good biocompatibility at room temperature (Karam and Abdurrahman, 2022; Acharya *et al*., 2021). ZnONPs exhibit remarkable antibacterial, antifungal, photocatalytic, and antioxidant activities, and they have been extensively explored for applications in drug delivery, bioimaging, molecular diagnostics, and wound healing (Odeomelam *et* al., 2023; Yang *et al*., 2023; Truong *et al*., 2023). These physicochemical properties make ZnO nanoparticles particularly suitable as nano-adsorbents for the removal of toxic metal ions from aqueous environments. Furthermore, their favorable optical, electrical, and semiconducting characteristics make ZnONPs suitable for use in advanced solar cells, biosensors, electronic and optoelectronic devices, as well as laser technologies, resulting in widespread application across various industrial and research sectors (Ahmad *et al*., 2020; Akintelu & Folorunso, 2020). Conventionally, ZnONPs have been synthesized using techniques such as hydrothermal processes, chemical vapor–liquid–solid deposition, metal–organic chemical vapor deposition, molecular beam epitaxy, sol–gel methods, microwave synthesis, laser ablation, chemical precipitation, and spray pyrolysis to meet increasing demand (Ahmad *et al.,* 2020; Rafique *et al.,* 2020). More recently, green synthesis approaches employing medicinal plant extracts have gained significant attention because of their simplicity, cost-effectiveness, safety, and environmental sustainability (Izein, 2024; Muresan *et al.*, 2024; Akintelu and Folorunso, 2020). Plant extracts are readily available, inexpensive, and rich in natural reducing and stabilizing agents, making them highly suitable for large-scale nanoparticle production (Karam & Abdurrahman, 2022).

Nanoparticles have a particle size within the range of 1 to 100 nm, at least in one dimension (Eddy *et* al., 2024a-c)). This dimension places them at an interface of material properties that are very unique for several outstanding properties and applications. For example, high surface area, large surface area to volume ratio, high porosity, tunable band gap, etc (Kelle *et al.*, 2023)

Among the numerous applications of nanotechnology, environmental remediation, particularly the removal of toxic heavy metals from contaminated water, has gained significant research attention because of nanoparticles exhibit size-dependent optical, electrical, and catalytic properties resulting from high surface-to-volume ratios (Adzu *et al.,* 2015; Ahmed & Mahmud, 2017). Their definition extends beyond conventional material emphasizing their behavior at the nanoscale. Heavy metal contamination of water resources poses serious environmental and public health risks due to toxicity, persistence, and bioaccumulation in living organisms.

The traditional method of water treatment often falls short in efficiently removing heavy metal pollutants. This has led to an increasing interest in exploring innovative and sustainable approaches, such as the use of nanoparticles for effective water remediation (Awual & Hasan, 2014)

ZnONPs have emerged as promising candidates for heavy metal removal due to their properties, including high surface area,

reactivity, and potential for surface modification. The green synthesis approach, utilizing natural extracts like *D. Mespillernis*, aligns with the growing emphasis on environmentally friendly and sustainable practices in nanotechnology (Bharathi *et al.*, 2018). Recent studies emphasize the growing relevance of adsorption-based nanomaterials for the removal of toxic heavy metals from wastewater. Al-Mur (2023) demonstrated that adsorption is the most efficient and economical wastewater treatment method compared to conventional approaches such as coagulation, membrane filtration, ion exchange, and biological treatment, which often suffer from high costs and limited efficiency. However, traditional adsorbents include. activated carbon, polymers, bio-based materials, industrial by-products, and zeolites are constrained by low adsorption capacity, poor selectivity, and limited active sites. To address these shortcomings, nanoparticles such as metal oxide nano-adsorbents have gained increasing attention. Zinc oxide (ZnO) nanoparticles stand out due to their high surface area, electron mobility, chemical stability, biocompatibility, low toxicity, and environmental friendliness. Green-synthesized ZnO nanoparticles derived from *Avicennia marina* leaf extract were reported to be spherical in shape, with an average size of ~29.1 nm and exhibited strong potential for adsorption removal of Cd^{2+} and Pb^{2+} from aqueous solution/

Complementarily, Kumar *et al*. (2024) highlighted the severe health risks associated with lead and cadmium, including bioaccumulation, nephrotoxicity, neurotoxicity, and carcinogenic effects, even at low exposure levels, underscoring the urgent need for effective remediation strategies. While biochar was identified as a promising, low-cost, and eco-friendly adsorbent due to its porous structure and modifiable surface chemistry, its practical application is limited by variable adsorption performance, competitive ion interference, slow kinetics, potential metal desorption, and scalability challenges. In contrast, ZnO nanoparticles offer superior adsorption efficiency owing to their high surface reactivity, tunable surface functional groups, and ease of dispersion within porous matrices. Adsorption studies characterized by FE-SEM and FT-IR revealed that Cd^{2+} and Pb^{2+} removal using ZnO nanoparticles is strongly pH-dependent and best described by pseudo-second-order kinetics and the Langmuir isotherm, indicating chemisorption on homogeneous surfaces.

Further supporting the potential of green nanotechnology, Durumin Iya *et al.* (2025) reported the successful green synthesis of ZnO nanoparticles using *Ixora coccinea* leaf extract for Co (II) removal, achieving a maximum removal efficiency of 83.8% at pH 10.3. FT-IR analysis confirmed the role of plant-derived phytochemicals in nanoparticle stabilization, while SEM verified nanoscale morphology. These findings reinforce that plant-mediated ZnO nanoparticle synthesis aligns with green chemistry principles by minimizing toxic reagents, reducing energy consumption, and improving cost-effectiveness. Overall, the literature strongly supports ZnO-based nano-adsorbents, either alone or in combination with biochar, as efficient, sustainable, and scalable alternatives for heavy-metal removal from wastewater. Green synthesis involves using environmentally benign materials and processes to produce nanoparticles. *D. mepiliformis* extract offers a green alternative to traditional chemical methods, reducing the environmental impact associated with nanoparticle synthesis (Dangoggo *et al.,* 2012) Heavy metals such as lead, cadmium, and mercury pose serious health risks even at trace concentrations. The effectiveness of ZnONPs synthesized using *D. mepiliformis* extract in removing these contaminants needs to be explored and validated.

Diospyros mespiliform is (commonly known as African ebony or "Kanya" in Hausa) is a savannah tree widely distributed across Africa. The plant contains diverse phytochemicals with reducing and stabilizing properties, making it a suitable candidate for green nanoparticle synthesis (Kanya in Hausa), a large deciduous tree found mainly in savannahs of Africa. It is a tall tree that grows up to 25 meters in height. It has a dense evergreen canopy. *D. Mespiliformis* (in italics) has been used in traditional medical systems, including Ayurveda, Chinese and African (Adzu *et al.,* 2022). The plant is widely used in parts of Africa and a number chemical constituents of therapeutic importance have been isolated. *D. Mespiliformis* has range of medicinal uses (Adzu *et al.,* 2015). A traditional food plant in potential to improve nutrition. This review article is aimed at compiling the pharmacological activities, phytochemical constituents and Ethnomedicinal uses. *D. Mespillernis*, commonly known as the African Ebony, possesses bioactive compounds with reducing and stabilizing properties. These compounds, including tannins, flavonoids, and polyphenols, have the potential to serve as effective natural agents in the synthesis of ZnONP (Bradl, 2005).

Despite the increasing number of studies on plant-mediated synthesis of ZnO nanoparticles, limited research has explored the use of *Diospyros mespiliformis* leaf extract as a reducing and stabilizing agent for ZnO nanoparticle production and its application in Pb(II) adsorption. Furthermore, the adsorption performance of biosynthesized ZnO nanoparticles derived from this plant remains insufficiently investigated. solutions. Therefore, this study aims to synthesize zinc oxide nanoparticles using *Diospyros mespiliformis* leaf extract through a green synthesis route and to evaluate their physicochemical characteristics and efficiency in removing Pb(II) ions from aqueous solution. The study shall contribute to green nanotechnology by integrating environmentally friendly nanoparticle synthesis with sustainable wastewater remediation. The utilization of a locally available plant resource can offer a cost-effective and eco-compatible strategy for heavy-metal removal, supporting circular and sustainable chemical practices.

2.0 Materials and Methods

2.1 Collection of samples

Fully matured leaves of *Diospyros mespiliformis* were collected from the Old Male Mosque area of Federal University Dutse (11°34′14.7″ N, 9°22′23.1″ E), Jigawa State, Nigeria, in November 2023. The collected leaves were thoroughly washed with tap water, followed by deionized water to remove dust and surface contaminants (Durumin Iya *et al.,* 2025). The leaves were shade-dried at room temperature for seven days to remove moisture while preserving bioactive constituents.

2.2 Preparation of the sample

The dried leaves were ground into a fine powder. Nanoparticle formation was indicated by the appearance of a pale-yellow precipitate. A 0.45 M NaOH solution was added dropwise to enhance precipitation and adjust alkalinity. The colloidal solution was then heated on a hot plate for 1 hour with constant stirring, where the pale yellowish precipitate changed into a deep yellow color/. The obtained precipitate was calcined in air to promote crystallization of ZnO nanoparticles. The particles were washed repeatedly with distilled water followed by ethanol to remove impurities, dried in an oven at 80 °C for 1 h, and ground into fine powder using a glass rod before storage in a sterile container for further characterization (Bharathi *et al*., 2018).

2.4 Characterization of the ZnONPs

The optical properties of the biosynthesized ZnO nanoparticles were analyzed using UV–Visible spectroscopy within the wavelength range of 320–800 nm. Functional groups

present on the nanoparticle surface were identified using Fourier Transform Infrared Spectroscopy (FTIR, PerkinElmer Spectrum 65) within the scanning range of 400–5000 cm^{-1}.

2.5 Water contamination

All chemicals used were of analytical grade and used without further purification.

Lead-contaminated water was prepared by dissolving lead nitrate [$Pb(NO_3)_2$] in distilled water to obtain a 0.1 M solution. The pH was adjusted to 7.0 using dilute H_2SO_4 and KOH solutions.

2.6 Adsorption studies

Adsorption experiments were conducted by mixing 0.1 g of ZnO nanoparticles with 20 mL of 0.10 mol dm^{-3} $Pb(NO_3)_2$ solution at room temperature. The adsorption experiment was carried out at a controlled pH of 7. The effect of initial metal ion concentration was investigated using Pb^{2+} solutions of 40, 50, 60, 70, and 80 mg L^{-1}.

The mixtures were centrifuged at 4000 rpm for 20 minutes to separate the adsorbent from the solution. The residual concentration of Pb^{2+} ions in the supernatant was determined using atomic absorption spectrophotometry (AAS) to evaluate adsorption efficiency and equilibrium time.

The equilibrium adsorption capacity, q_e (mg/g), which represents the amount of Pb^{2+} adsorbed per unit mass of the ZnO nanoparticles, was calculated using the mass balance relationship shown in equation 1 (Ogoko *et al*., 2023b)

$$q_e = \frac{(C_0 - C_e)V}{m} \quad (1)$$

where C_0 and C_e are the initial and equilibrium concentration of the adsorbate, V is the volume of the solution and m is the mass of the adsorbate.

3.0 Results and Discussion

3.1nThe analysis of UV-visible spectrum

The UV-Visible absorption spectrum of the synthesized zinc oxide (ZnO) nanoparticles (Fig. 1) exhibits a prominent and well-defined excitonic absorption peak centered at 340 nm. This feature is characteristic of the intrinsic bandgap transition in ZnO, where electrons are excited from the valence band to the conduction band. Notably, the absorption maximum at 340 nm reflects a significant blue shift compared to the bulk ZnO absorption edge, which typically occurs around 370–380 nm. This hypochromic shift is a direct consequence of the quantum confinement effect, indicating that the particle dimensions are smaller than the Bohr exciton radius of the material. The sharpness of the peak further suggests a relatively narrow particle size distribution and high crystallinity within the sample.

The optical bandgap (E_{BG}) was evaluated using the Planck equation shown in equation 2 (Nuhu *et al*., 2025)

$$E_{BG} = \frac{hc}{\lambda_{max}} \quad (2)$$

where λ_{max} is the wavelength of maximum absorption (340 nm), h is the Planck constant and c is the speed of light in a vacuum. The calculation yielded an approximate value of 3.65 eV. This increased energy gap, relative to the bulk value of 3.37 eV, confirms the successful reduction of the material to the nanometric scale. Furthermore, the spectrum shows negligible absorption in the visible region above 400 nm, transitioning into a steep absorption edge in the ultraviolet region. This profile is consistent with the high transparency and potent UV-shielding properties required for multifaceted applications in optoelectronics and photocatalysis. The subtle tailing observed near the absorption edge may be attributed to minor polydispersity or the presence of shallow surface defects within the ZnO lattice.

The observed blue shift (340 nm vs. the bulk 370 nm) is the most critical indicator. In the context of adsorption, this shift

confirms the "quantum confinement effect," which only occurs when particles are extremely small. Smaller particles inherently possess a much higher specific surface area (SSA). Since adsorption is a surface-dependent phenomenon, the UV spectrum essentially "proves" that there is a vast landscape of available active sites for heavy metal ions to bind to, which would not be present in larger, bulkier particles.

3.2 Infrared Fourier Transform (FTIR) Analysis

The FTIR spectrum of the *D. mespiliformis* coarse powder (Fig. 2a) displays a variety of functional groups characteristic of secondary metabolites such as polyphenols, flavonoids, and proteins. 2is attributed to the O-H stretching vibrations of phenolic compounds and alcohols Khan *et al*., 2021; Siddiqi *et al.*, 2022). while the peaks at 2918 cm^{-1} and 2851 cm^{-1} correspond to C-H stretching in aliphatic chains (Elumalai *et al*., 2020). The presence of carbonyl groups (C=O) and aromatic C=C bonds is indicated by peaks in the 1734–1607 cm^{-1} range, suggesting the presence of carboxylic acids or esters. In the FTIR spectrum of the ZnO NPs (Fig. 2b), a significant shift and broadening of the O-H band to 3301 cm^{-1} is observed, indicating the involvement of hydroxyl groups in the reduction and stabilization process. The disappearance or reduction in intensity of the aliphatic C-H peaks (2918–2851 cm^{-1}) suggests that these components were either consumed or modified during the synthesis. Crucially, a new, sharp, and intense absorption band appears in the lower fingerprint region below 700 cm^{-1} (specifically around 672 cm^{-1}). This peak is the characteristic signature of the Zn-O stretching vibration, confirming the formation of the crystalline metal oxide lattice. The identified crystalline phases, along with their corresponding chemical formulas, JCPDS card numbers, and crystallographic information, are presented in Table 4.

The persistence of peaks at 1582 cm^{-1} and 1402 cm^{-1} in the nanoparticle spectrum indicates that the surface of the ZnO NPs is "capped" with biomolecules from the extract, which prevents agglomeration and enhances biocompatibility (Rajiv *et al.,* 2023).

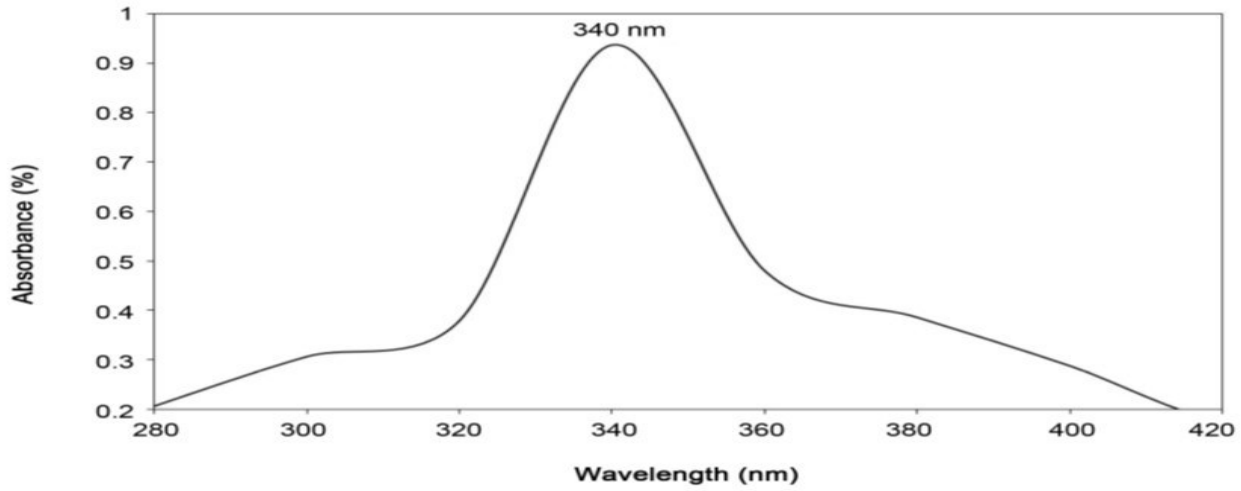

Fig. 1: UV-Vis spectrum of synthesized ZnO-NPs (Durumin Iya *et al.*, 2025)

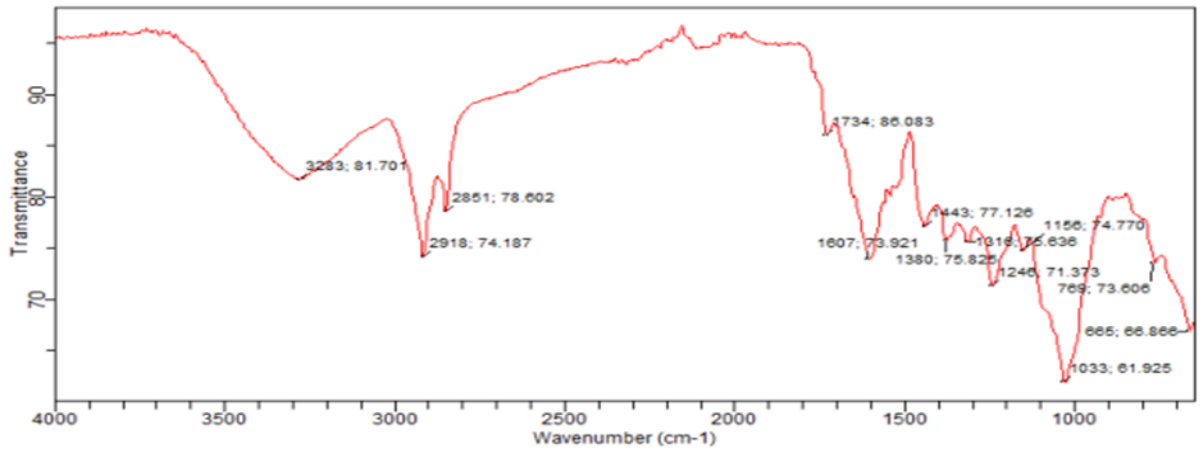

Fig. 2a: FTIR of fine coarse powder of *D. mespiliformis*

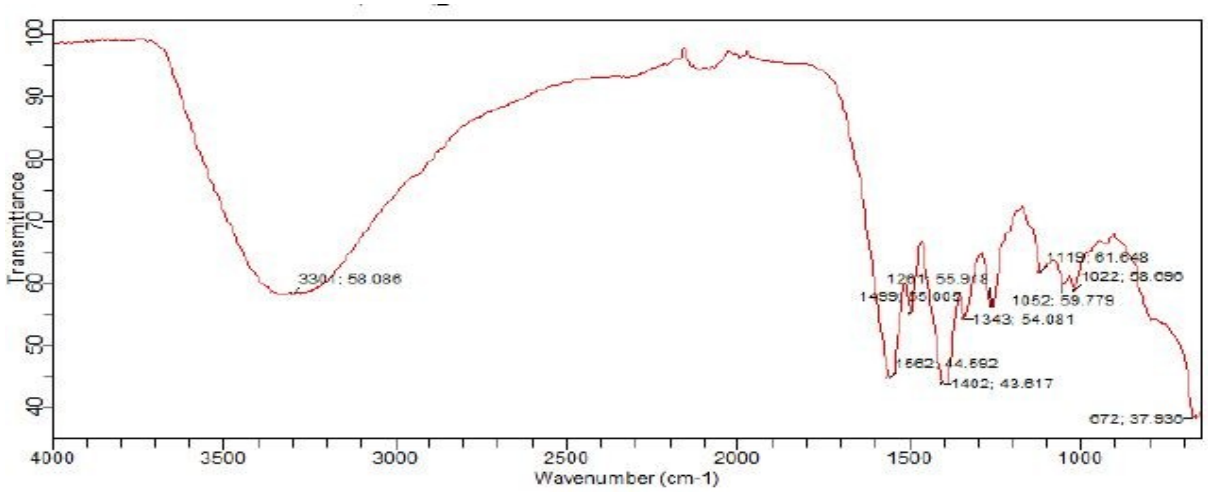

Fig. 2b: FTIR of Zinc Oxide nanoparticles

The FTIR data provide several key scientific justifications for the effectiveness of these "green" ZnO nanoparticles as superior adsorbents for heavy metal removal. The spectrum of the ZnO NPs (Fig. 2b) clearly demonstrates that the nanoparticles are not "naked" but are instead coated with residual plant-derived functional groups, including hydroxyls, carboxyl, and amines. These groups act as efficient chelating agents that form stable complexes with divalent heavy metal cations, such as Pb^{2+}, Cd^{2+}, and $Hg^{2+,}$ through coordination bonding. Furthermore, the broad hydroxyl (–OH) peak observed at 3301 cm^{-1} suggests a surface rich in oxygen-containing moieties, which, in aqueous solutions, can deprotonate to create a negatively charged surface. This high surface negativity facilitates the strong electrostatic attraction and subsequent removal of positively charged heavy metal ions from contaminated water. Additionally, the capping mechanism evidenced by the shifted aromatic and carbonyl peaks suggests that the biomolecules from *D. mespiliformis* provide a protective layer that inhibits particle growth and aggregation. By maintaining a smaller, discrete nanoparticle size, the material preserves the high specific surface area required to maximize the density

of available active adsorption sites per unit mass of the material (Daimari and Deka, 2024).

3.3 Scanning Electron Microscope (SEM)

The SEM micrographs (Fig. 3) reveal that the ZnO nanoparticles possess a predominantly granular and quasi-spherical morphology. At the observed magnifications, the surface appears highly textured and characterized by a porous, sponge-like architecture. This irregular and roughened surface is scientifically significant as it indicates a high degree of surface area, which aligns with the strong absorption observed in the UV-Vis spectra and the high density of functional groups identified via FTIR. The presence of these pores and surface irregularities provides a complex network of channels that can facilitate the diffusion and subsequent entrapment of heavy metal contaminants.

3.4 EDX analysis

The elemental composition and quantitative distribution of the biosynthesized ZnO nanoparticles were evaluated using Energy Dispersive X-ray (EDX) spectroscopy, and the results are presented in Fig. 4 and Table 1. The EDX data provide clear evidence of the successful formation of ZnO nanoparticles alongside the incorporation of residual elements originating from the plant extract and synthesis medium.

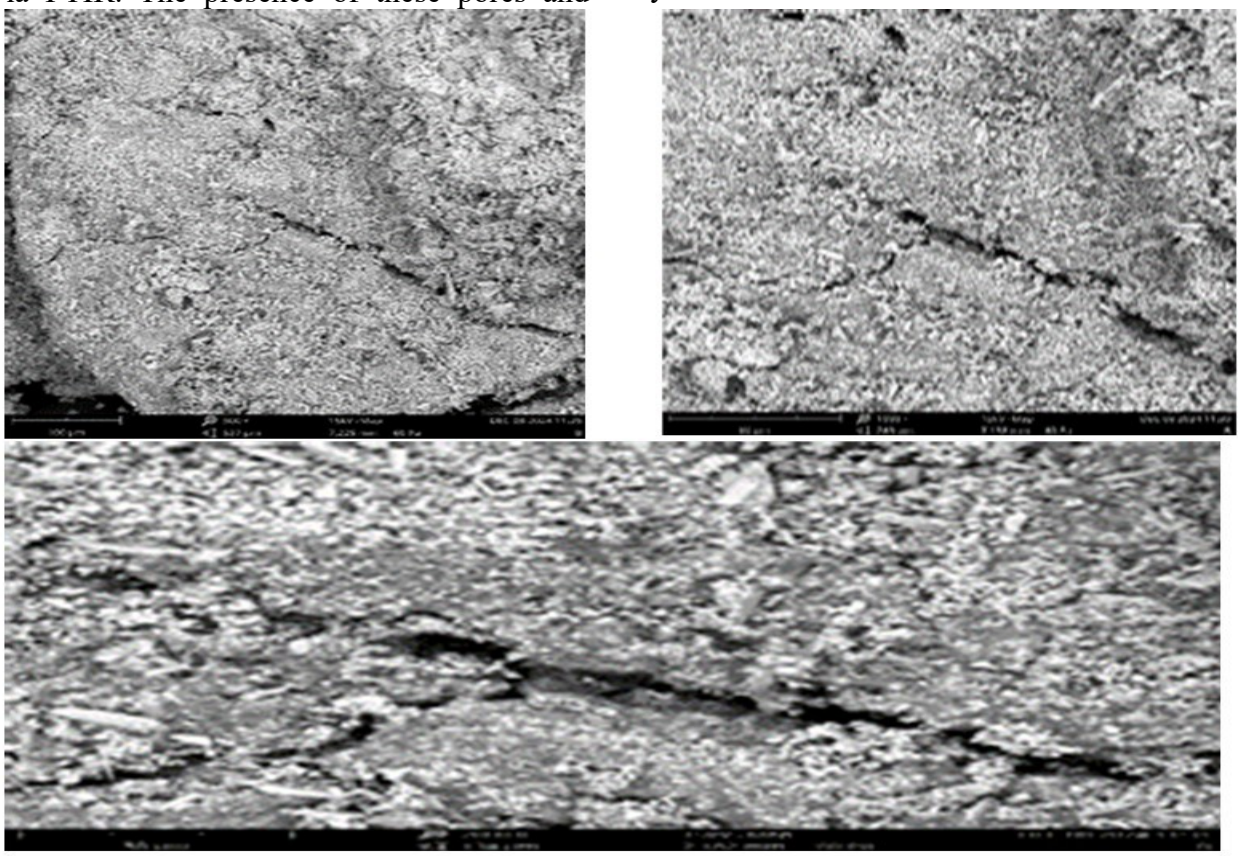

Fig. 3: The morphologies, shape and size of the ZnONPs

As shown in Table 1, Zinc (Zn), which is the principal constituent of ZnO, exhibits a weight concentration of 40.59% and an atomic concentration of 19.61%. This confirms the formation of the ZnO phase and is consistent with the characteristic Zn signals observed in the EDX spectrum, typically around 1.0 keV (Lα) and 8.6 keV (Kα). The relatively high Zn

content validates that the synthesized material is predominantly zinc-based, in agreement with the XRD results indicating Zincite as the dominant crystalline phase.

A notable feature of the EDX data is the exceptionally high sodium (Na) content, with 78.68% atomic concentration and 57.28% weight concentration. This can be attributed to the use of NaOH during synthesis as well as the natural abundance of sodium ions in the Diospyros mespiliformis leaf extract. The elevated Na content suggests possible surface adsorption or incorporation of sodium species within the nanoparticle matrix, which may contribute to surface charge development and enhance ion-exchange properties during adsorption processes.

In addition to Zn and Na, minor quantities of calcium (Ca), titanium (Ti), silicon (Si), potassium (K), chlorine (Cl), and phosphorus (P) were detected, each with weight percentages below 1.5%. These trace elements are typical of green synthesis routes and originate from intrinsic plant biomolecules and environmental precursors. Their presence indicates that the nanoparticles are not purely inorganic but rather exist as bio-functionalized nanostructures. Elements such as Ca and K, being alkali and alkaline earth metals, can introduce exchangeable surface sites, thereby improving the affinity of the nanoparticles for divalent heavy metal ions through ion-exchange mechanisms.

Furthermore, the detection of Si and Ti suggests slight incorporation of mineral impurities or lattice defects, which can play a significant role in modifying the electronic and surface properties of ZnO. These defects may act as active centers for adsorption by increasing surface reactivity and facilitating surface complexation reactions. The presence of Cl and P in trace amounts further supports the involvement of phytochemical residues and possible precursor salts used during synthesis.

From a technical perspective, the EDX results strongly support the multifunctional nature of the synthesized ZnO nanoparticles. The combination of a ZnO core with a surface enriched in bio-derived elements and inorganic ions creates a heterogeneous interface that is highly favorable for adsorption. The high sodium content, in particular, suggests that ion-exchange mechanisms may significantly contribute to Pb^{2+} removal, where Na^{+} ions are replaced by heavier metal ions in solution. Additionally, the presence of multiple trace elements and associated lattice imperfections enhances the density of active sites, thereby promoting chemisorption and electrostatic interactions.

The EDX analysis confirms not only the successful synthesis of ZnO nanoparticles but also reveals a complex, bio-functionalized surface chemistry that is directly responsible for the enhanced adsorption performance observed in this study.

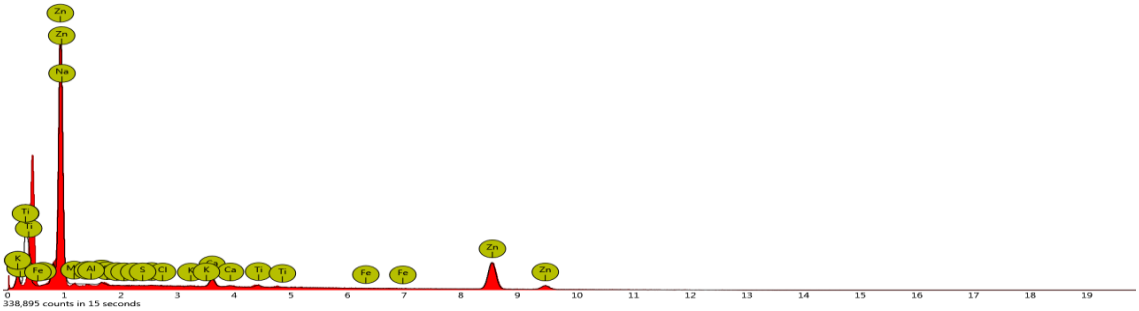

Fig. 4: Showing the composition of elements present in ZnO-NPs

Table 1: Elemental Composition of ZnO Nanoparticles as Determined by Energy Dispersive X-ray (EDX) Analysis

Element Name	Element Symbol	Element Number	Atomic Conc. (%)	Weight Conc. (%)
Sodium	Na	11	78.68	57.28
Zinc	Zn	30	19.61	40.59
Calcium	Ca	20	1.02	1.29
Titanium	Ti	22	0.30	0.46
Silicon	Si	14	0.26	0.23
Potassium	K	19	0.06	0.08
Chlorine	Cl	17	0.04	0.04
Phosphorus	P	15	0.03	0.03

Memory full

The EDX results are highly consistent with the previously discussed UV-Vis and FTIR data, confirming the inorganic identity of the core material while supporting the presence of a complex bio-organic hybrid surface. From a technical standpoint, this elemental variety provides strong evidence for the material's superior adsorption capacity. The presence of inherent bio-minerals such as Na, K, and Ca suggests a surface rich in ion-exchangeable sites, where these "soft" cations can be readily displaced by "harder" heavy metal contaminants like Pb^{2+}, Cd^{2+} and Hg^{2+} in aqueous solutions. Furthermore, the inclusion of trace transition metals like Titanium and Iron indicates a doped or defective crystal lattice. Such defects, as suggested by the tailing in the UV-Vis spectrum, function as high-energy active centers that facilitate the chemical anchoring and surface complexation of heavy metal ions.

3..5 XRD Profile

The X-ray diffraction pattern shown in Fig. 5 provides comprehensive information on the phase composition, crystallinity, and structural integrity of the biosynthesized ZnO nanoparticles. The diffraction peaks are sharp and well-defined, indicating a high degree of crystallinity, while the presence of multiple reflections confirms the polycrystalline and multiphase nature of the material. The dominant peaks observed at 2θ ≈31.7 34.4, and 36.68 ° correspond to the (100), (002), and (101) crystallographic planes of hexagonal wurtzite ZnO, which are in excellent agreement with the standard JCPDS Card No. 00-001-1136. The high intensity and sharpness of these peaks confirm that Zincite constitutes the major crystalline phase, accounting for 83 wt% of the material, as presented in Table 2. Additional diffraction peaks corresponding to Gahnite ($ZnAl_2O_4$) and Cristobalite (SiO_2) match well with JCPDS Card No. 00-001-1146 and JCPDS Card No. 00-001-0424, respectively, confirming the multiphase composition of the sample.

The interplanar spacing (d) corresponding to the observed diffraction peaks was calculated using Bragg's law given in equation (3) (Eddy *et al*., 2023c)

$$d_{spacing} = \frac{n}{2sin\theta} \qquad (3)$$

where n = 1, λ=1.5406 A˚ and θ is the Bragg angle. For the peak at 2θ=36.68◦, corresponding to Gahnite (101), the calculated $d_{spacing}$ is 2.448 Å, which is in close agreement with the standard reference value of approximately 2.44 Å Similarly, for the peak at 2θ = 56.99◦ , attributed to Cristobalite (331), the calculated dd-spacing of 1.614 Å compares well with the standard value of about 1.60 Å.

Minor deviations between experimental and standard d-spacing values are observed and can be attributed to lattice strain, crystallite size effects, instrumental broadening, and the incorporation of foreign ions or defects into the crystal lattice during the green synthesis process. In particular, the presence of biomolecules and trace elements identified in the EDX analysis can induce slight distortions in the lattice parameters, leading to peak shifts and variations in interplanar spacing. The calculated crystallite size, full width at half maximum (FWHM), and interplanar spacing values derived from the representative diffraction peaks are summarized in Table 3.

The crystallite size of the nanoparticles was estimated using the Debye–Scherrer equation shown in Equation (4) (Eddy *et al*., 2024a-c)

$$d_{cryst} = \frac{k\lambda}{\beta cos\theta} \qquad (4)$$

where d_{cryst} is the crystallite size, l = 0.9., λ = 0.15406 nm, β is the full width at half maximum in radians, and θ is the Bragg angle.

The calculated crystallite sizes of 13.7 nm for Gahnite and 8.6 nm for Cristobalite confirm the nanoscale dimension of the material. The relatively small crystallite sizes and peak broadening further indicate the presence of micro strain, which was evaluated using equation (5)

$$\varepsilon = \frac{\beta}{4tan\theta} \qquad (5)$$

The calculated strain values suggest moderate lattice distortion, which is characteristic of nanoparticles synthesized via biological routes. Additionally, the dislocation density, which represents the defect concentration within the crystal, was estimated using equation (6):

$$\delta = \frac{1}{d_{crysy}^2} \qquad (6)$$

The relatively high dislocation density values confirm that the nanoparticles possess a defect-rich structure. These structural imperfections, including vacancies, interstitials, and grain boundaries, play a crucial role in enhancing surface reactivity.

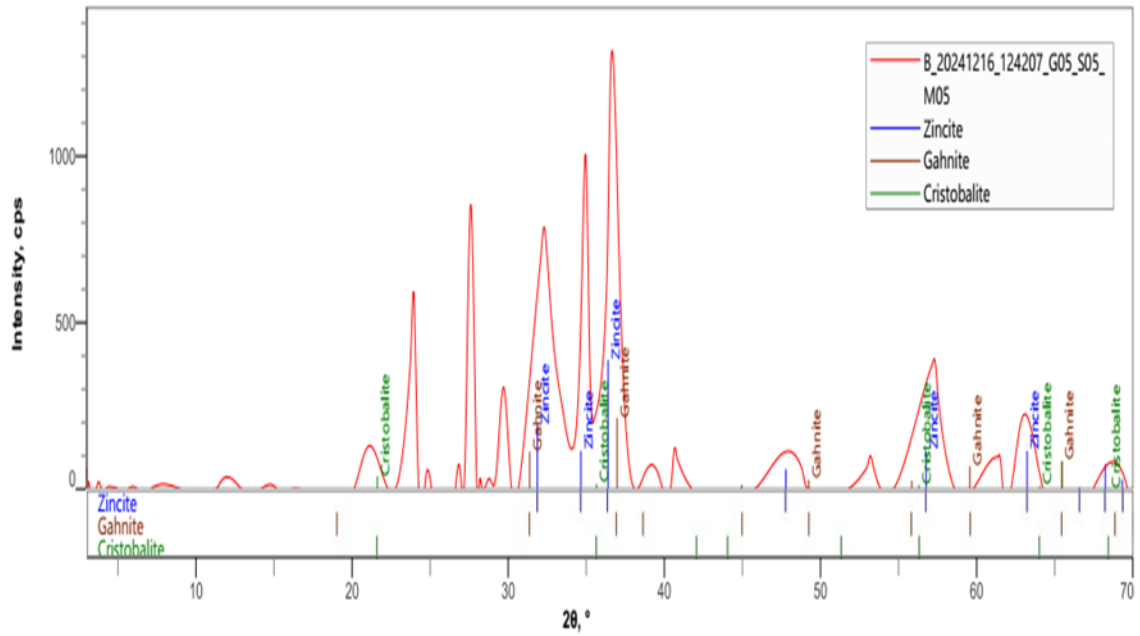

Fig. 5: Shows the results of X-ray Diffraction of ZnO-NPs

Table 2 Title: Presence and Proportions of Crystalline Phases

S/N	Phase	Weight (%)	Interpretation
1	Zincite	83	Confirming that ZnO is the principal crystalline phase
2	Gahnite	13	Attributed to a solid-state reaction between ZnO and Al_2O_3 at elevated temperatures
3	Cristobalite	3.8	Likely due to silica impurities or high-temperature transformation of quartz

Table 3 Title: Characteristics of Two Different Diffraction Peaks

Parameter	Peak at 2θ = 36.68°	Peak at 2θ = 56.99°
Phase	Gahnite	Cristobalite
Estimated Crystallite Size	137 Å (≈ 13.7 nm)	86 Å (≈ 8.6 nm)
Miller Index	101	331
Full Width at Half Maximum (FWHM)	0.64	1.10
Interplanar Spacing (d)	2.448 Å	1.614 Å

Comparison with standard reference data shows that while the peak positions closely match the JCPDS patterns, slight peak shifts and broadening are evident. Such deviations are commonly reported in green-synthesized ZnO nanoparticles and are primarily due to quantum size effects, incorporation of impurities such as Na, Ca, and Si, and the influence of capping agents from the plant extract. These factors collectively introduce lattice distortion and reduce long-range crystallographic order, resulting in a semi-crystalline structure.

The implications of these structural features for adsorption are significant. The reduced crystallite size increases the specific surface area, thereby providing a larger number of active sites for metal ion adsorption. The observed lattice strain and high dislocation density create defect sites that act as high-energy adsorption centers, facilitating strong interactions with Pb^2. Furthermore, the multiphase composition involving ZnO, $ZnAl_2O_4$, and SiO_2 enhances surface heterogeneity, which promotes multiple adsorption mechanisms, including electrostatic attraction, ion exchange, and surface complexation. The slight deviation in ddd-spacing also suggests altered surface electronic environments, which can improve the binding affinity of the nanoparticles toward heavy metal ions.

Overall, the XRD analysis confirms that the synthesized ZnO nanoparticles possess a highly crystalline yet defect-rich and heterogeneous structure, with nanoscale crystallite size and slight lattice distortions. These characteristics are highly advantageous for adsorption applications, as they collectively enhance surface reactivity, increase the density of active sites, and improve the overall efficiency of heavy metal removal from aqueous systems.

3.6. Adsorption Studies of Heavy Metals and Mechanistic Synthesis

3.6.1. Effect of Initial Metal Ion Concentration

The initial concentration of metal ions serves as a critical driving force to overcome mass transfer resistance between the aqueous and solid phases. The adsorption of Pb(II) onto the biosynthesized ZnO nanoparticles was

evaluated across a concentration range of 5 to 25 mg/L, as detailed in Table 5. The data indicates that as the initial concentration of Pb(II) increased from 0.346 mg/L to 1.268 mg/L, the removal efficiency generally improved, achieving a notable maximum of 78.39% at an intermediate concentration of 0.574 mg/L. This trend suggests that at these concentrations, the active sites on the ZnO NPs are highly available and efficiently utilized. The slight fluctuations in removal percentage at the highest concentrations may be attributed to the progressive saturation of the available adsorption sites on the fixed 0.05 g dosage of the adsorbent.

Table 4 Title: Identified Crystalline Phases and Structural Parameters

Phase Name	Formula	Card Number	Group Spacing	Quantity (wt%)
Zincite	**ZnO**	**00-001-1136**	**186: P63mc**	**83**
Gahnite	**$ZnAl_2O_4$**	**00-001-1146**	**227: Fd-3:2**	**13**
Cristobalite	**SiO_2**	**00-001-0424**	**227: Fd-3:2**	**3.8**

Table 5: Effect of Initial Concentration on Pb^{2+} Removal by ZnO NPs

S/N	Initial Conc. (mg/L)	Residual Conc. (mg/L)	% Metal Removal
1	0.346 ± 0.0098	0.166 ± 0.0561	52.02
2	0.504 ± 0.0143	0.190 ± 0.0227	62.30
3	0.574 ± 0.0182	0.124 ± 0.0661	78.39
4	0.985 ± 0.1687	0.373 ± 0.0169	62.13
5	1.268 ± 0.1365	0.292 ± 0.0706	77.97

3.6.2. Effect of Solution pH

The pH of the solution is a pivotal parameter in adsorption studies as it dictates both the speciation of the metal ions and the surface charge of the adsorbent. As shown in Table 6, the removal efficiency of Pb^{2+} demonstrated a strong pH dependency, increasing significantly from 21.5% at pH 2.3 to a maximum of 83.8% at pH 10.3. At low pH values, the high concentration of hydrogen ions competes with Pb(II) cations for adsorption sites, and the protonation of surface functional groups leads to electrostatic repulsion. As the pH increases toward alkaline conditions, the deprotonation of surface hydroxyl and carboxyl groups—identified previously in the FTIR analysis—results in a negatively charged surface, thereby enhancing the electrostatic attraction and removal of the positively charged lead ions.

Table 6: Influence of pH on Pb^{2+} Adsorption Efficiency

S/N	pH of Solution	% Metal Removal
1	2.3	21.5
2	4.1	35.6
3	6.2	44.9
4	8.1	61.3
5	10.3	83.8

3.6.3. Synthesis of Characterization and Adsorption Results

The superior adsorption performance of the synthesized ZnO nanoparticles is deeply rooted in the synergistic agreement between the various characterization techniques employed. The UV-Vis analysis confirmed the nanometric scale and quantum confinement of the particles, which translates to the high specific surface area visible in the SEM micrographs.

This physical architecture provides the necessary "spatial capacity" for high-volume contaminant sequestration.

Chemically, the FTIR results confirmed that the nanoparticles are capped with bioactive functional groups (–OH and C=O) from *D. mespiliformis*, providing the specific chelating sites required for the 78–83% removal efficiencies observed in the adsorption trials. This is further supported by the EDX and XRD data; the presence of Zincite as the major phase ensures a high density of reactive ZnO centers, while the secondary phases (Gahnite and Cristobalite) and trace bio-minerals (Na, K, Ca) introduce structural defects and ion-exchange sites. These defects, evidenced by the crystallite sizes of 8.6–13.7 nm, serve as high-energy anchors for heavy metals. Collectively, the results demonstrate that the "green" synthesis route not only produces stable ZnO nanoparticles but specifically engineers a multi-functional surface ideally suited for the remediation of Pb(II) from aqueous environments.

4.0 Conclusion

The aim of the study was achieved, whereby the ZnO NPs were synthesized from aqueous extract of *D. mespiliformis*, the morphology was determined using FT-IR spectroscopy and Scanning Electron microscope (SEM). The efficacy of biosynthesized nanoparticles on the removal of Pb (ii) in water was analyzed using Atomic Absorption Spectroscopy (AAS). The ZnO nanoparticles, derived from *D. mespiliformis* extract, exhibit notable characteristics conducive to effective Pb^{2+} removal. The multifaceted mechanisms involved in this process, including adsorption and potential chemical interactions, contribute to the overall efficacy of the nanoparticles in water treatment. Moreover, the eco-friendly nature of *D. mespiliformis* extract as a reducing and capping. agent adds to the sustainability aspect of the synthesized ZnO nanoparticles. This not only addresses the issue of water pollution but also aligns with the growing emphasis on green and sustainable technologies. The successful removal of lead ions signifies a practical application of the synthesized nanoparticles in addressing environmental challenges. As we move forward. further exploration of the scalability, long-term stability, and potential synergies with existing water treatment methods will be crucial.

In conclusion, the synthesis of ZnO nanoparticles using *D. mespiliformis* extract present a promising avenue for advancing water purification technologies, with implications for sustainable and effective solutions to mitigate the impact of lead contamination in water sources.

5.0 References

Abegunde, S. M., Adebayo, M. A., & Olasehinde, E. F. (2024). Green synthesis of ZnO nanoparticles and its application for methyl green dye adsorption. *Green Energy & Resources*, 2, 100073. https://doi.org/10.1016/j.gerr.2024.100073

Acharya, T. R., Lamichhane, P., Wahab, R., Chaudhary, D. K., Shrestha, B., Joshi, L. P., Kaushik, N. K., & Choi, E. H. (2021). Study on the synthesis of ZnO nanoparticles using Azadirachta indica extracts for the fabrication of a gas sensor. *Molecules*, 26, 24, 7685. https://doi.org/10.3390/molecules26247685

Adzu, O. T., Mohamed, F., Naidoo, Y., Adu, T. S., Chenia, H., Dewir, Y. H., & Rihan, H. (2022). Green synthesis of silver nanoparticles from Diospyros villosa extracts and evaluation of antioxidant, antimicrobial and anti-quorum sensing potential. *Plants*, 11, 19, 2514. https://doi.org/10.3390/plants11192514

Adzu, B., Chindo, B. A., Tarfa, F. D., Salawu, O. A., & Igoli, O. J. (2015). Isolation and analgesic property of lupeol from D.

mespiliformis stem bark. *Journal of Medicinal Plants Research*, 9, 30, pp. 813–819. https://doi.org/10.5897/JMPR2015.5877

Ahmad, H., Venugopal, K., Rajagopal, K., De Britto, S., Nandini, B., Pushpalatha, H. G., Konappa, N., Udayashankar, A. C., Geetha, N., & Jogaiah, S. (2020). Green synthesis and characterization of zinc oxide nanoparticles using Eucalyptus globulus and their fungicidal ability against pathogenic fungi of apple orchards. *Biomolecules*, 10, 3, 425. https://doi.org/10.3390/biom10030425

Ahmed, A., & Mahmud, A. (2017). Pharmacological activities of D. mespiliformis: a review. *J Pharm Biol Sci*, 7, pp. 93–96

Akintelu, S. A., & Folorunso, A. S. (2020). A review on green synthesis of zinc oxide nanoparticles using plant extracts and its biomedical applications. *BioNanoScience*, 10, pp. 848–863. https://doi.org/10.1007/s12668-020-00774-6

Al-Mur, B. A. (2023). Green zinc oxide (ZnO) nanoparticle synthesis using mangrove leaf extract from avicenna marina: properties and application for the removal of toxic metal ions (Cd2+ and Pb2+). *Water*, 15, 3, 455

Asmat-Campos, D., López-Medina, E., Montes de Oca-Vásquez, G., Gil-Rivero, E., Delfín-Narciso, D., Juárez-Cortijo, L., Villena-Zapata, L., Gurreonero-Fernández, J., & Rafael-Amaya, R. (2022). ZnO nanoparticles obtained by green synthesis as an alternative to improve the germination characteristics of L. esculentum. *Molecules*, 27, 7, 2343. https://doi.org/10.3390/molecules27072343

Awual, M. R., & Hasan, M. M. (2014). Novel conjugate adsorbent for visual detection and removal of toxic lead (II) ions from water. *Microporous and Mesoporous Materials*, 196, pp. 261–269. https://doi.org/10.1016/j.micromeso.2014.05.021

Azizi, S., Ahmad, M. B., Namvar, F., & Mohamad, R. (2014). Green biosynthesis and characterization of zinc oxide nanoparticles using brown marine macroalga Sargassum muticum aqueous extract. *Materials Letters*, 116, pp. 275–277. https://doi.org/10.1016/j.matlet.2013.11.038

Azizi, S., Mohamad, R., & Mahdavi Shahri, M. (2017). Green microwave-assisted combustion synthesis of zinc oxide nanoparticles with Citrullus colocynthis (L.) Schrad: characterization and biomedical applications. *Molecules*, 22, 2, 301. https://doi.org/10.3390/molecules22020301

Bergström, L., Rosseeva, S. E. V., Salazar-Alvarez, G., & Cölfen, H. (2015). Mesocrystals in biominerals and colloidal arrays. *Acc Chem Res*, 48, 5, pp. 1391–1402. https://doi.org/10.1021/ar500440b

Bharathi, D., Josebin, D. M., Vasantharaj, S., & Bhuvaneshwari, V. (2018). Biosynthesis of silver nanoparticles using stem bark extracts of Diospyros montana and their antioxidant and antibacterial activities. *Journal of Nanostructure in Chemistry*, 8, pp. 83–92. https://doi.org/10.1007/ s40097-018-0256-7

Bhattacharjee, N., Som, I., Saha, R., & Mondal, S. (2024). A critical review on novel eco-friendly green approach to synthesize zinc oxide nanoparticles for photocatalytic degradation of water pollutants. *Int J Environ Anal Chem*, 104, 3, pp. 489–516. https://doi.org/10.1080/03067319.2021.2022130

Bradl, H. (2005). Sources and origins of heavy metals. In Interface science and technology, Vol. 6, pp. 1-27: Elsevier. https://doi.org/10.1016/S1573-4285(05)80020-1

Daimari, J., & Deka, A. K. (2024). Anticancer, antimicrobial and antioxidant activity of CuO–ZnO bimetallic nanoparticles: green synthesized from Eryngium foetidum leaf extract. *Scientific Reports*, 14, 19506. https://doi.org/10.1038/s41598-024-69847-w

Dangoggo, S., Hassan, L., Sadiq, I., & Manga, S. (2012). Phytochemical analysis and antibacterial screening of leaves of D. mespiliformis and Ziziphus spina-christi. Journal of Chemical Engineering, 1(1), 31–37.

Durumin Iya, N. I., Yunusa, F. A., Olaleye, A., Badamasi, H., Eri, S. M., & Yahaya, A. (2025). Green synthesis of ZnO nanoparticles using Ixora coccinea leaf extract for efficient removal of Co (II) from water. *UMYU Scientifica*, 4, 3, pp. 144–153. https://doi.org/10.56919/usci.2543.014

Eddy, N. O., Garg, R., Garg, R., Aikoye, A., & Ita, B. I. (2023c). Waste to resource recovery: mesoporous adsorbent from orange peel for the removal of trypan blue dye from aqueous solution. *Biomass Conversion and Biorefinery*, 13, pp. 13493–13511. https://doi.org/10.1007/s13399-022-02571-5

Eddy, N. O., Odiongenyi, A. O., Garg, R., Ukpe, R. A., Garg, R., El Nemr, A., Ngwu, C. M., & Okop, I. J. (2023a). Quantum and experimental investigation of the application of Crassostrea gasar (mangrove oyster) shell–based CaO nanoparticles as adsorbent and photocatalyst for the removal of procaine penicillin from aqueous solution. *Environmental Science and Pollution Research*, 30, 23, pp. 64036–64057. https://doi.org/10.1007/s11356-023-26868-8

Eddy, N. O., Ukpe, R. A., Ameh, P., Ogbodo, R., Garg, R., & Garg, R. (2023b). Theoretical and experimental studies on photocatalytic removal of methylene blue (MetB) from aqueous solution using oyster shell synthesized CaO nanoparticles (CaONP O). *Environmental Science and Pollution Research*. https://doi.org/10.1007/s11356-022-22747-w

Eddy, N. O., Garg, R., Ukpe, R. A., Ameh, P. O., Gar, R., Musa, R., Kwanchi, D., Wabaidur, S. M., Afta, S., Ogbodo, R., Aikoye, A. O., & Siddiqu, M. (2024c). Application of periwinkle shell for the synthesis of calcium oxide nanoparticles and in the remediation of Pb^{2+}-contaminated water. *Biomass Conversion and Biorefinery*. https://doi.org/10.1007/s13399-024-05285-y

Eddy, N. O., Jibrin, J. I., Ukpe, R. A., Odiongenyi, A., Iqbal, A., Kasiemobi, A. M., Oladele, J. O., & Runde, M. (2024b). Experimental and theoretical investigations of photolytic and photocatalysed degradations of crystal violet dye (CVD) in water by oyster shells derived CaO nanoparticles (CaO-NP). *Journal of Hazardous Materials Advances*, 13, 100413. https://doi.org/10.1016/j.hazadv.2024.100413

Eddy, N. O., Oladede, J., Eze, I. S., Garg, R., Garg, R., & Paktin, H. (2024a). Synthesis and characterization of CaO nanoparticles from periwinkle shell for the treatment of tetracycline-contaminated water by adsorption and photocatalyzed degradation. *Results in Engineering*, 103374. https://doi.org/10.1016/j.rineng.2024.103374

El-Saadony, M. T., Fang, G., Yan, S., Alkafaas, S. S., El Nasharty, M. A., Khedr, S. A., Hussien, A. M., Ghosh, S., Dladla, M., Elkafas, S. S., Ibrahim, E. H., Salem, H. M., Mosa, W. F., Ahmed, A. E., Mohammed, D.

M., Korma, S. A., El-Tarabily, M. K., Saad, A. M., El-Tarabily, K. A., & AbuQamar, S. F. (2024). Green synthesis of zinc oxide nanoparticles: preparation, characterization, and biomedical applications - a review. *Int J Nanomedicine*, 19, pp. 12889–12937. https://doi.org/10.2147/IJN.S487188

Elumalai, K., Velmurugan, S., Ravi, S., Kathiravan, V., & Ashokkumar, S. (2015). Green synthesis of zinc oxide nanoparticles using Moringa oleifera leaf extract and evaluation of its antimicrobial activity. *Spectrochimica Acta Part A*, 143, pp. 158–164. https://doi.org/10.1016/j.saa.2015.02.011

Fouda, A., Saied, E., Eid, A. M., Kouadri, F., Alemam, A. M., Hamza, M. F., Alharbi, M., Elkelish, A., & Hassan, S. E. D. (2023). Green synthesis of zinc oxide nanoparticles using an aqueous extract of Punica granatum for antimicrobial and catalytic activity. *Journal of Functional Biomaterials*, 14, 4, 205. https://doi.org/10.3390/jfb14040205

Jadhav, V., Roy, A., Kaur, K., Rai, A. K., & Rustagi, S. (2024). Recent advances in nanomaterial-based drug delivery systems. *Nano-Structures and Nano-Objects*, 37, pp. 101–103. https://doi.org/10.1016/j.nanoso.2024.101103

Karam, S. T., & Abdulrahman, A. F. (2022). Green synthesis and characterization of ZnO nanoparticles by using thyme plant leaf extract. *Photonics*, 9, 8, 594. https://doi.org/10.3390/photonics9080594

Karan, T., Gonulalan, Z., Erenler, R., Kolemen, U., & Eminagaoglu, O. (2024). Green synthesis of silver nanoparticles using Sambucus ebulus leaves extract: Characterization, quantitative analysis of bioactive molecules, antioxidant and antibacterial activities. *Journal of Molecular Structure*, 1296, 136836. https://doi.org/10.1016/j.molstruc.2023.136836

Kelle, H. I., Ogoko, E. C., Akintola, O., & Eddy, N. O. (2023). Quantum and experimental studies on the adsorption efficiency of oyster shell–based CaO nanoparticles (CaONPO) towards the removal of methylene blue dye (MBD) from aqueous solution. *Biomass Conversion and Biorefinery*, 14, pp. 31925–31948. https://doi.org/10.1007/s13399-023-04947-7

Khan, I., Saeed, K., & Khan, I. (2019). Nanoparticles: Properties, applications and toxicities. *Arabian Journal of Chemistry*, 12, pp. 908–931. https://doi.org/10.1016/j.arabjc.2017.05.011

Kumar, V., Sable, H., Singh, V., Pandit, S., & Ranjan, N. (2024). Mitigation of lead (Pb^{2+}) and cadmium (Cd^{2+}) synthetic wastewater using Datura metal fruit peel biochar-zinc oxide nanocomposite. Research Square

Latif, A., Mohsin, M., Bhatti, I. A., Tahir, A. A., Hussain, M. T., & Iqbal, J. (2023). Experimental and ab initio studies of Co-doped ZnO nano photocatalyst thin films. *RSC Advances*, 13, pp. 35003–35016. https://doi.org/10.1039/D3R A04491B

Izein, B. (2024). Nano revolution: Tiny tech, big impact: How nanotechnology is driving SDGs progress. *Heliyon*, 10, 10, e31393, pp. 1–26. https://doi.org/10.1016/j.heliyon.2024.e31393

Mahdavi, M., Ahmad, M. B., Haron, M. J., Ab Rahman, M. Z., & Azizi, S. (2012). Rapid removal of Cu (II) ion by chemically modified rubber wood fiber. *Environmental Engineering Science*, 29, 2, pp. 1–7. https://doi.org/ 10.1089/ees.2011.0129

Mahdavi, S., Jalali, M., & Afkhami, A. (2012). Removal of heavy metals from aqueous solutions using Fe_3O_4, ZnO, and CuO nanoparticles. *Journal of Nanoparticle*

Research, 14, 8, 846. https://doi.org/10.1007/S11051-012-0846-0

Morowvat, M. H., Kazemi, K., Jaberi, M. A., Amini, A., & Gholami, A. (2023). Biosynthesis and antimicrobial evaluation of zinc oxide nanoparticles using Chlorella vulgaris biomass against multidrug-resistant pathogens. *Materials*, 16, 2, 842. https://doi.org /10.3390/ma16020842

Muresan, E. I., Pui, A., Cernatescu, C., Cimpoesu, R., Horhogea, C. E., Istrate, B., & Rîmbu, C. M. (2024). Green synthesis of nanoparticles containing zinc complexes and their incorporation in topical creams with antimicrobial properties. *Applied Sciences*, 14, 11, 4612. https://doi.org/10.3390/app1411 4612

Nuhu, J. S., Awe, F. E., Garg, R., Garg, R., Eddy, N. O., & Paktin, H. (2025). Cobalt titanate nanocatalyst for enhanced photodegradation of atrazine: Kinetics, degradation efficiency, and mechanistic analysis. *BMC Chemistry*, 19, 31. https://doi.org/10.1186/s13065-025-01394-5

Odoemelam, S. A., Oji, E. O., Eddy, N. O., Garg, R., Garg, R., Islam, S., Khan, M. A., Khan, N. A., & Zahmatkesh, S. (2023). Zinc oxide nanoparticles adsorb emerging pollutants (glyphosate pesticide) from aqueous solution. *Environmental Monitoring and Assessment*. https://doi.org/10.1007/s10661-023-11255-0

Ogoko, E. C., Kelle, H. I., Akintola, O., & Eddy, N. O. (2023). Experimental and theoretical investigation of Crassostrea gigas shells based CaO nanoparticles as a photocatalyst for the degradation of bromocresol green dye (BCGD) in an aqueous solution. *Biomass Conversion and Biorefinery*. https://doi.org/10.1007/s13399-023-03742-8

Prashanth, G. K., Dileep, M. S., Gadewar, M., Ghosh, M. K., Rao, S., Giresha, A. S., Prashanth, P. A., Swamy, M. M., Yatish, K. V., & Mutthuraju, M. (2024). Zinc oxide nanostructures: Illuminating the potential in biomedical applications: A brief overview. *BioNanoScience*, 14, pp. 1876–1896. https://doi.org/10.1007 /s12668-024-01366-4

Rafique, M., Tahir, R., Gillani, S. S. A., Tahir, M. B., Shakil, M., Iqbal, T., & Abdellahi, M. O. (2020). Plant-mediated green synthesis of zinc oxide nanoparticles from Syzygium cumini for seed germination and wastewater purification. *Int J Environ Anal Chem*, 102, pp. 23–38. https://doi.org/10.1080/03067319.2020.171537

Rajiv, P., Bavadharani, B., Kumar, M. N., & Vanathi, P. (2017). Synthesis and characterization of biogenic iron oxide nanoparticles using green chemistry approach and evaluating their biological activities. *Biocatalysis and Agricultural Biotechnology*, 12, pp. 45–49. https://doi.org/10.1016/j.bcab .2017.08.015

Ramteke, R. D., Hemrick, J. G., & Mahapatra, M. K. (2025). Phase formation in the CaO–Al_2O_3–ZnO system as an analogue to CaO–Al_2O_3–MgO in spinel containing refractories. *J Am Ceram Soc*, 108, e20393. https://doi.org/ 10.1111/jace.20393

Salayová, A., Bedlovičová, Z., Daneu, N., Baláž, M., Bujňáková, Z. L., Balážová, Ľ., & Tkáčiková, L. (2021). Green synthesis of silver nanoparticles with antibacterial activity using various medicinal plant extracts: Morphology and antibacterial efficacy. *Nanomaterials*, 11, 4, 1005. https://doi. org/10.3390/nano11041005

Sedefoglu, N. (2024). Green synthesis of ZnO nanoparticles by Myrtus communis plant extract with investigation of effect of precursor, calcination temperature and study of photocatalytic performance. *Ceramics International*, 50, pp. 9884–9895

Seghir, B. B., Hima, M., Moulatti, F., Sahraoui, I., Ben Amor, I., Zeghoud, S., Hemmami, H., Kouadri, I., Ben Amor, A., Messaoudi, M., Ahmed, S., Rebiai, A., & Pohl, P. (2023). Exploring the antibacterial potential of green-synthesized MgO and ZnO nanoparticles from two plant root extracts. *Nanomaterials*, 13, 17, 2425. https://doi.org/10.3390/nano13172425

Siddiqi, K. S., Ur Rahman, A., Tajuddin, N., & Husen, A. (2018). Properties of zinc oxide nanoparticles and their activity against microbes. *Nanoscale Research Letters*, 13, 1, 141. https://doi.org/10 .1186/s11671-018-2532-3

Sugitha, S. K. J., Venkatesan, R., Latha, R. G., Vetcher, A. A., Al-Asbahi, B. A., & Kim, S.-C. (2024). A study on the antibacterial, antispasmodic, antipyretic, and anti-inflammatory activity of ZnO nanoparticles using leaf extract from Jasminum sambac (L. Aiton). *Molecules*, 29, 7, 1464. https://doi.org/10.3390/molecules29071464

Truong, T. T., Khieu, T. T., Luu, H. N., Truong, H. B., Nguyen, V. K., Vuong, T. X., & Tran, T. K. N. (2023). Characterization and bioactivity of Piper chaudocanum L. extract-doped ZnO nanoparticles biosynthesized by co-precipitation method. *Materials*, 16, 15, 5457. https://doi.org/10.3390/ma16155457

Yang, X., Cao, X., Chen, C., Liao, L., Yuan, S., & Huang, S. (2023). Green synthesis of zinc oxide nanoparticles using aqueous extracts of Hibiscus cannabinus L.: Wastewater purification and antibacterial activity. *Separations*, 10, 9, 466. https://doi.org/10.3390/separations10090466

Declaration

Consent for publication

Not Applicable

Availability of data and materials

The publisher has the right to make the data public

Ethical Considerations

Not applicable

Competing interest

The authors report no conflict or competing interest

Funding

The authors declared no source of funding

Author Contributions

Naseer Inuwa Durumin Iya conceptualized the study, supervised the research, and finalized the manuscript. Ishak Haladu, Abba Yahaya and Fatima Abdulkarim Yunusa collected samples and carried out the laboratory analyses. Hafiz Ahmad, Musa Muhammad Bello and Aminu Bala performed SEM-EDX and XRD.